

Upper Mid-Band Channel Measurements and Characterization at 6.75 GHz FR1(C) and 16.95 GHz FR3 in an Indoor Factory Scenario

Mingjun Ying^{†1}, Dipankar Shakya^{†2}, Theodore S. Rappaport^{†3},
Peijie Ma[†], Yanbo Wang[†], Idris Al-Wazani[†], Yanze Wu[†], and Hitesh Poddar*
[†]*NYU WIRELESS, Tandon School of Engineering, New York University, USA*
**Sharp Laboratories of America (SLA), Vancouver, Washington, USA*
{¹yingmingjun, ²dshakya, ³tsr}@nyu.edu

Abstract—This paper presents detailed radio propagation measurements for an indoor factory (InF) environment at 6.75 GHz and 16.95 GHz using a 1 GHz bandwidth channel sounder. Conducted at the NYU MakerSpace in the NYU Tandon School of Engineering campus in Brooklyn, NY, USA, our measurement campaign characterizes a representative small factory with diverse machinery and open workspaces across 12 locations, comprising 5 line-of-sight (LOS) and 7 non-line-of-sight (NLOS) scenarios. Analysis using the close-in (CI) path loss model with a 1 m reference distance reveals path loss exponents (PLE) below 2 in LOS at 6.75 GHz and 16.95 GHz, while in NLOS PLE is similar to free-space propagation. The RMS delay spread (DS) decreases at higher frequencies with a clear frequency dependence. Similarly, RMS angular spread (AS) measurements show wider spreads in NLOS compared to LOS at both frequency bands, with a decreasing trend as frequency increases. These observations in a dense-scatterer environment demonstrate frequency-dependent behavior that deviate from existing industry-standard models. Our findings provide crucial insights into complex propagation mechanisms in factory environments, essential for designing robust industrial wireless networks at upper mid-band frequencies.

Index Terms—FR3, FR1(C), 6G, InF, factory, upper mid-band, delay spread, angular spread, path loss, propagation, channel model

I. INTRODUCTION

The increasing demand for higher data rates, lower latency, and enhanced reliability in wireless communication systems has driven the exploration of new frequency bands, such as FR1(C) (4-8 GHz) and FR3 (7-24 GHz). These upper mid-band frequencies offer a promising middle ground between coverage and capacity, providing wider bandwidth than the Sub-6 GHz spectrum while avoiding some of the propagation challenges associated with millimeter-wave (mmWave) frequencies. Regulatory agencies, such as ITU and FCC, have identified these bands as key candidates for future 5G and 6G deployments in urban and industrial environments [1], [2].

While significant research has focused on the higher mmWave and sub-terahertz (sub-THz) bands [3], there is still a

limited understanding of the propagation characteristics in industrial environments, where wireless signals face distinct challenges. Unlike urban outdoor or indoor office spaces, factories often include diverse metallic surfaces, heavy machinery, and dynamic obstacles, which make propagation conditions more complex due to increased reflection, scattering, and diffraction effects. The propagation characteristics in these environments must be well understood to develop robust wireless systems for industrial applications [4], [5].

Previous studies have demonstrated the unique propagation behavior in industrial environments. For example, Rappaport et al. [6], [7] conducted pioneering measurements at 1.3 GHz in factory settings, reporting a path loss exponent (PLE) of 2.15, highlighting the need for dedicated channel models for factory environments. At higher frequencies, Schmiieder et al. [8] found that at 28 GHz in industrial spaces, blockage significantly affects the LOS component, though it has a limited impact on overall channel gain.

Recent studies have explored various industrial environments across different frequency bands to better understand wireless channel characteristics. Vijayan et al. [9] conducted 5G channel measurements in a medical device manufacturing facility, focusing on the challenges posed by metallic structures. Using a simulated environment at 3.6 GHz, authors in [9] reported satisfactory channel gains despite the significant reflections caused by the metallic infrastructure, which increased multipath effects. In another study, Al-Samman et al. [10] performed wideband measurements at 107-109 GHz in manufacturing halls and test rooms. Their study revealed PLE ranging from 1.6 to 1.9 and a substantial increase in delay spread in NLoS conditions, emphasizing the need for optimized designs in such high-frequency scenarios.

Further research by Wang et al. [11] examined channel characteristics in micro-drilling and milling areas at 28 GHz. Their results indicated a PLE of 1.41 in LOS conditions and 2.81 in NLOS conditions. Additionally, they observed significant angular spread and delay spread, suggesting that propagation characteristics in industrial environments at mmWave frequencies are more complex due to dense multipath components (MPCs).

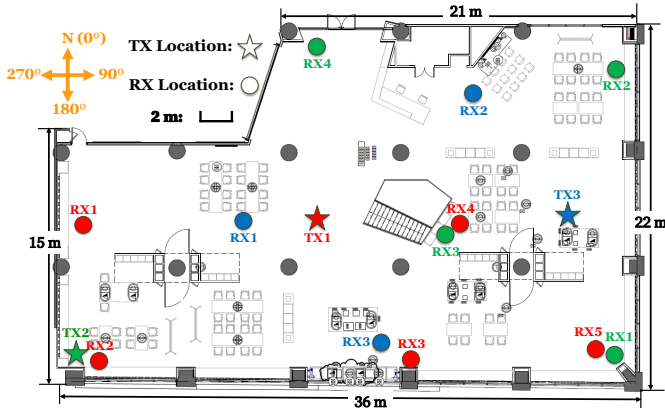


Fig. 1: Floor plan of NYU MakerSpace factory environment showing three TX locations (★) and their associated RX positions (●), with matching colors indicating TX-RX pairs.

Meanwhile, Lyczkowski et al. [12] studied the propagation behavior in automated guided vehicle lanes across frequencies from 2.1 GHz to 5.1 GHz. They reported notably small NLOS PLE values that increased with frequency, showing values ranging from 1.12 to 2.56. Their work highlights the variability of propagation characteristics in industrial environments as frequency increases, especially in the presence of obstacles like heavy machinery.

This work presents a detailed empirical study of channel measurements at 6.75 GHz and 16.95 GHz within the NYU MakerSpace factory environment, focusing on critical metrics such as path loss, delay spread, angular spread, and polarization. The remainder of this paper is organized as follows: Section II describes the channel sounder, the indoor factory environment, and the measurement procedures. Section III presents a comprehensive analysis of channel characteristics at 6.75 GHz and 16.95 GHz, including path loss modeling for co-polarized and cross-polarized antenna configurations, directional and omnidirectional path loss models, a comparison of delay and angular spreads across different environments and frequencies, and a comparison with the standardized values from 3GPP TR 38.901 [13]. Finally, Section IV summarizes the key findings of this paper.

II. CHANNEL MEASUREMENT IN INF WITH A 1 GHz BANDWIDTH CHANNEL SOUNDER

A. Channel Sounding System

A sliding correlation-based wideband channel sounder, detailed in [14], [15], was used for channel propagation measurements. The system generated a 500 Mcps PN sequence at baseband, upconverted to a 1 GHz wideband RF signal at 6.75 GHz for FR1(C) and further upconverted to 16.95 GHz for FR3 using a heterodyne architecture. The RX employed a slightly slower 499.9375 Mcps PN sequence, resulting in a time-dilated PDP due to the sliding correlation.

The unique feature of this sounder, as highlighted in [16], is its dual-band co-located design, which allows seamless switching between 6.75 GHz and 16.95 GHz by changing

the IF signal cable to the appropriate RF module. Detailed specifications of the sounder system are provided in [16]–[18].

B. Calibration of the Channel Sounder System

The calibration procedure ensures accurate power, delay, and direction capture of multipath components (MPC). The complete calibration comprises three phases:

1) *Linearity and Power Calibration*: The linear range of operation and system gain is confirmed by measuring the transmit power using a Keysight N1913A power meter and the N8487A power sensor. The TX power is kept within the FCC’s 35 dBm licensed limit. Free-space path loss (FSPL) measurements at a distance beyond five times the far-field (D_f) of the horn antennas verify system gain and correct attenuator settings. A 4 m separation at 1.5 m TX and RX height ensures a single LOS path for accurate calibration, adhering to [19]. The linearity and power calibration are conducted twice daily at the start and end of the day to ensure accurate capture of MPCs throughout the day.

2) *Time Calibration*: To ensure accurate multipath delay measurement, the two Rubidium (Rb) clocks at the TX and RX are first synchronized overnight using a physical cable. Each day, during system startup, Raspberry Pi computers connected to the Rb clocks initiate a Precision Time Protocol (PTP) synchronization to continually synchronize the two Rb clocks when the physical cable is disconnected for untethered measurements [20]. After linearity calibration, the LOS peak in the PDP is circular-shifted to match the free-space propagation delay for the 4 m calibration distance. After each location’s measurement, the TX and RX return to their calibration spots to remeasure the LOS path, to compensate for any minor drift in propagation delay accumulated during the long-duration measurement sessions.

Unlike previous campaigns, this setup continuously synchronizes the Rb clocks and PDPs using patent-pending methods [20], eliminating the need for post-processing or ray-tracing corrections to the time drift.

3) *Spatial Calibration*: At each TX-RX location, antennas are mounted at 2.4 m (TX) and 1.5 m (RX) heights, using geographical North as the 0-degree reference for spatial coordination. Once calibration (system linearity, time, and space) is complete, the channel sounder is ready for propagation measurements [16].

C. Indoor Factory Environment

The NYU MakerSpace Factory, approx. 36 m × 22 m × 5 m (W×L×H), is an active manufacturing space equipped with a variety of machinery, including several 3D printers, CNC machines, laser cutters, PCB fabrication and soldering stations, metal and woodwork stations, and few robotic arms. The Factory’s exterior walls on the north, south, and east sides were covered by large glass panels framed with metal, creating reflective surfaces, while the west wall consisted of thick drywall.

During channel measurements, 3 TX locations and 12 RX locations were used, with the TX placed at a height of 2.4

TABLE I: TX-RX location pairs for factory InF measurements at 6.75 GHz in FR1(C) and 16.95 GHz in FR3 [16]

TX	Loc Type	RX	T-R Separation (m)
TX1	LOS	RX1	14.6
		RX4	9
	NLOS	RX2	16.6
		RX3	11.1
		RX5	19
TX2	LOS	RX1	33.3
		RX3	24.9
	NLOS	RX2	38.2
		RX4	24.6
TX3	LOS	RX1	19.3
	NLOS	RX2	9.5
		RX3	14

m, and the RX at 1.5 m. Concrete pillars (represented as gray-filled circles in Fig. 1) were positioned throughout the space, impacting the MPCs propagation. Alongside the pillars, the various machines and material surfaces contributed to the complex scattering environment.

The TX-RX location pairs for the 6.75 GHz FR1(C) and 16.95 GHz FR3 measurements are listed in Table I, including 5 LOS and 7 NLOS TX-RX pairs, with separations ranging from 9 m to 38 m. At full power, our measurement system has a link margin of 155.6 dB at 6.75 GHz and 159.2 dB at 16.95 GHz [16], [21], [22]. However, to stay within FCC license requirements, a max EIRP of 31 dBm is used during field measurements to achieve a practical link margin of 142.7 dB at 6.75 GHz and 143.8 dB at 16.95 GHz [23], which results in no outages at any location.

D. Measurement Procedure

The measurements at the TX-RX locations follow a systematic approach as highlighted:

- Rapid RX azimuth scans identify significant TX angles of departure (AODs) [16].
- Detailed RX azimuthal sweeps in half-power beamwidth (HPBW) steps conducted for each AOD identified by the rapid scans following Table II.
- Measurements in both co-polarized and cross-polarized antenna configurations.
- Calibration before and after measurements at each location for temporal and spatial accuracy.

III. 6.75 AND 16.95 GHz INF RADIO PROPAGATION CHARACTERISTICS

A. Path Loss

The measured path loss obtained from the directional and omnidirectional PDPs is fit to the CI model with a 1 m free space reference distance, d_0 , to evaluate the path loss exponent (PLE or n).

$$PL^{CI}(f_c, d_{3D}) \text{ [dB]} = \text{FSPL}(f_c, 1\text{m}) + 10n \log_{10} \left(\frac{d_{3D}}{d_0} \right) + \chi_{\sigma}, \quad (1)$$

$$\text{FSPL}(f_c, 1\text{m}) = 32.4 + 20 \log_{10} \left(\frac{f_c}{1 \text{ GHz}} \right),$$

where $\text{FSPL}(f_c, 1 \text{ m})$ is obtained for carrier frequency f_c GHz at 1 m, n is the PLE, and χ_{σ} is large-scale shadow fading (zero-mean Gaussian r.v. with s.d. σ^{CI} in dB) [24].

TABLE II: TX/RX elevation configurations for 360° azimuthal sweeps at fixed TX angles [16]

Sweep #	TX elevation	RX elevation	
1	TX at boresight elevation.	RX at boresight elevation, then swept 360° in azimuth plane in HPBW [†] steps.	
2		RX tilted down by one HPBW [†] , then swept 360° in azimuth plane in HPBW steps.	
3		RX tilted up by one HPBW [†] , then swept 360° in azimuth plane in HPBW steps.	
4		TX tilted down by one HPBW [†] .	RX at boresight elevation, then swept 360° in azimuth plane in HPBW steps.
5		TX tilted down by one HPBW [†] .	RX tilted down by one HPBW [†] , then swept 360° in azimuth plane in HPBW steps.

[†]HPBW: 30° @ 6.75 GHz; 15° @ 16.95 GHz.

Fig. 2 shows the directional CI PL models and scatter plots for co-polarized antennas in an InF environment at 6.75 GHz and 16.95 GHz. The measurements cover T-R separations from 9 to 38 m. The PLE is evaluated for three cases: LOS, NLOS_{Best}, and NLOS. The NLOS_{Best} PL is calculated for the NLOS RX pointing in the direction of the highest received power. The LOS PLE at 6.75 GHz is 1.64, with NLOS_{Best} and NLOS PLEs at 2.22 and 2.92. At 16.95 GHz PLEs of 2.09, 2.48, and 3.81 are seen for LOS, NLOS_{Best}, and NLOS.

After synthesizing the omnidirectional PDPs using the method described in [25], we observe a lower PLE at 6.75 GHz, measuring 1.39 in LOS and 1.78 in NLOS, compared to 16.95 GHz, where the PLE values are 1.75 in LOS and 2.11 in NLOS. The low PLE at 6.75 GHz may be attributed to the structural characteristics of the MakerSpace, which includes plasterboard or wooden partitions with open sections at the top or bottom, facilitating easier penetration of lower-frequency waves. The relatively low PLE in NLOS at 6.75 GHz suggests a quasi-line-of-sight (QLOS) scenario, as defined in [26], where partial obstructions allow for some signal diffraction around obstacles, yielding a PLE less than 2, unlike fully obstructed NLOS conditions. Additionally, the absence of permanent walls contributes to the reception of scattered power from multiple directions at NLOS locations. The frequency comparison in Table III further highlights the trend of increasing PLE at higher frequencies.

3GPP does not include a CI model option for path loss in InF environments; instead, it uses the Floating Intercept (FI) model, as specified in *Table 7.4.1-1: Path Loss Models* in [13]. The FI model also varies the y-intercept as a fitting parameter and does not use a physical reference of the free-space propagation as in the CI model. Furthermore, 3GPP classifies the factory environment for TX heights above the surrounding clutter as sparse clutter-high height (SH) and dense clutter-high height (DH). Models for both classifications are shown in Table III.

B. RMS Delay Spread

The RMS DS provides a measure of the temporal spread of MPCs in the environment. A power threshold of 25 dB

TABLE III: Directional and Omnidirectional CI PL model (FI model for 3GPP) parameters for 6.75 GHz FR1(C) and 16.95 GHz FR3 InF campaigns, with comparison to 142 GHz campaign in [27]

Campaign	Distance (m)	Antenna HPBW (TX/RX)	Directional path loss						Omni path loss			
			LOS		NLOS Best		NLOS		LOS		NLOS	
			n	σ (dB)	n	σ (dB)	n	σ (dB)	n	σ (dB)	n	σ (dB)
6.75 GHz (This work)	9-38	(30°/30°)	1.64	1.44	2.22	3.88	2.92	7.69	1.39	1.86	1.78	2.46
6.75 GHz (3GPP)	10-600	–	–	–	–	–	–	–	$n:2.15$ $\alpha:31.84$	4.3	$n_{SH}:2.3$ $\alpha_{SH}:32.4$ $n_{DH}:2.19$ $\alpha_{DH}:33.63$	$SH:5.9$ $DH:4$
16.95 GHz (This work)	9-38	(15°/15°)	2.09	6.2	2.48	4.2	3.81	10.42	1.75	3.1	2.11	3.29
16.95 GHz (3GPP)	10-600	–	–	–	–	–	–	–	$n:2.15$ $\alpha:31.84$	4.3	$n_{SH}:2.3$ $\alpha_{SH}:32.4$ $n_{DH}:2.19$ $\alpha_{DH}:33.63$	$SH:5.9$ $DH:4$
142 GHz [27]	9-38	(8°/8°)	2.1	1.8	3.12	7.1	4.92	11.3	1.86	2.2	2.74	5.1

Notation: SH = Sparse clutter and High base station height (Tx or Rx elevated above the clutter), DH = Dense clutter and High base station height.

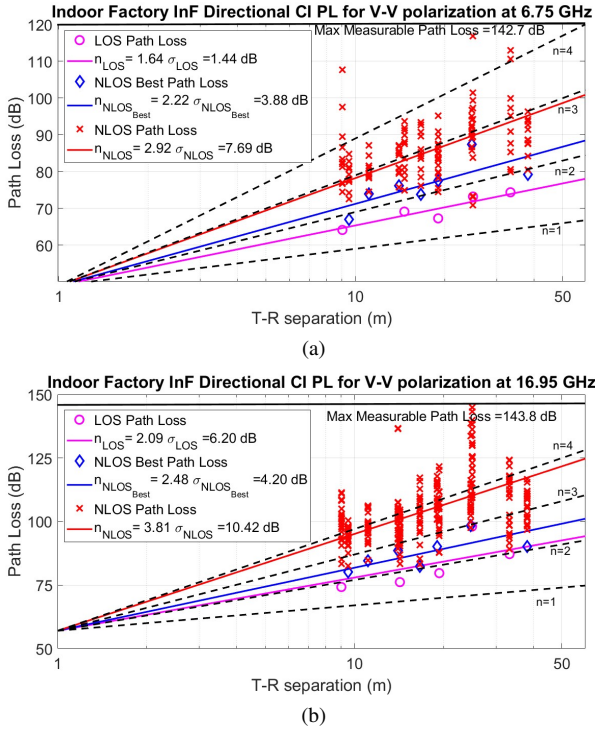


Fig. 2: InF directional CI PL models and scatter plot for V-V polarization at: (a) 6.75 GHz FR1(C); (b) 16.95 GHz FR3. [T-R separation: 9–38 m]

below the peak or 5 dB above the noise floor is used to evaluate the RMS DS. Table IV presents the RMS DS at the two frequencies, along with the 3GPP results from *Table 7.5-6 Part-3: Channel Model Parameters for InF* in [13]. The mean values are evaluated in log-scale and the expectations are calculated assuming underlying log-normal distribution for a direct comparison with 3GPP. NLOS RMS DS is clearly observed decreasing with frequency, LOS RMS DS is observed similar with slightly higher DS at 16.95 GHz, compared to 6.75 GHz. In LOS, the omnidirectional RMS DS is obtained as 14 ns at 6.75 GHz and 12.7 ns at 16.95 GHz, while in NLOS RMS DS is observed as 30.3 ns at 6.75 GHz and 29 ns at 16.95 GHz.

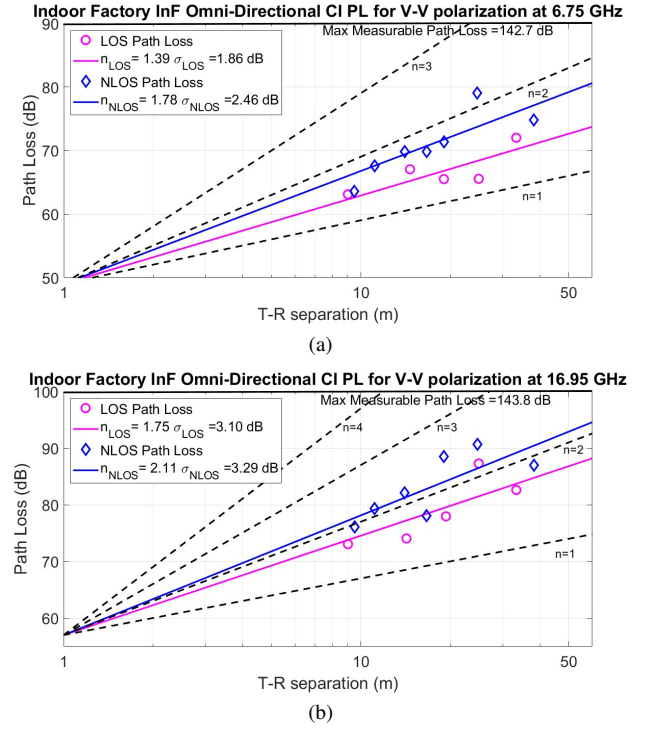


Fig. 3: InF omnidirectional CI PL models and scatter plot for V-V polarization at: (a) 6.75 GHz FR1(C); (b) 16.95 GHz FR3. [T-R separation: 9–38 m]

The RMS DS in the 3GPP model depends on the physical dimensions of the environment, particularly the volume (V) and enclosing surface area (S) considering the walls, ceiling and floor, rather than the frequency [13]. For the NYU MakerSpace floorplan shown in Fig. 1, the V is calculated as 3470 m³ and the S as 1958 m², assuming a uniform height of 5 m.

C. RMS Angular Spread

The RMS AS shows the spatial dispersion of arrival or departure angles in azimuth and elevation planes. RMS AS is evaluated for a spatial lobe threshold of 10 dB below the strongest pointing direction, using procedures detailed in [22]. Table V summarizes the AS observed for both arrival angles

TABLE IV: RMS Delay Spread Characteristics from 6.75 GHz to 142 GHz for LOS and NLOS Conditions.

Frequency (GHz)	6.75	6.75 (3GPP)	16.95	16.95 (3GPP)	142 [27]
Dir RMS DS					
LOS	11.2	–	13.7	–	1.8
$\mathbb{E}(\cdot)$ (ns)					
NLOS	11.3	–	9.2	–	3.2
$\mathbb{E}(\cdot)$ (ns)					
Omni RMS DS					
LOS	14	26.84	12.7	26.84	5.5
$\mathbb{E}(\cdot)$ (ns)					
NLOS	30.3	30.92	29.0	30.92	11
$\mathbb{E}(\cdot)$ (ns)					

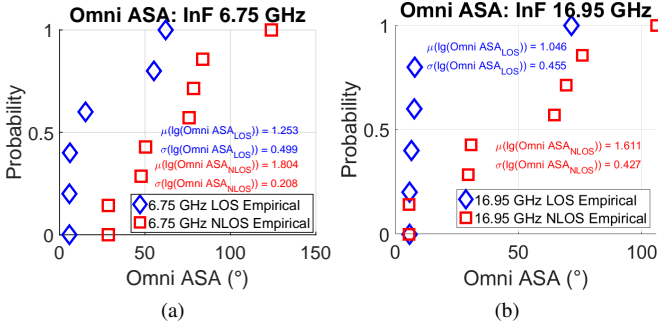


Fig. 4: InF omnidirectional ASA: (a) 6.75 GHz; (b) 16.95 GHz. [T-R separation: 9–38 m]

at the RX (ASA) and departure angles at the TX (ASD). In LOS, the ASA is observed as 23.71° at 6.75 GHz and 14.32° at 16.95 GHz. Wide ASAs of 66.38° and 50.40° are observed in NLOS at 6.75 GHz and 16.95 GHz, respectively. 3GPP models a frequency-dependent LOS ASA with overestimated spread, along with a constant NLOS ASA, as outlined in *Table 7.5-6 Part-3: Channel Model Parameters for InF* and *Table 7.5-11: ZSD and ZOD Offset Parameters for InF* in [13]. ASAs are observed to decrease with frequency in both LOS and NLOS. Further, the ASDs are observed as 35.89° in LOS and 45.93° in NLOS at 6.75 GHz, while ASDs of 22.91° in LOS and 34.77° in NLOS are observed at 16.95 GHz. As shown in Fig. 4, the CDFs of empirical data align with these trends, while 3GPP predictions suggest a constant ASD of 39° in LOS and 38.9° in NLOS across frequencies.

Point data for large-scale spatio-temporal parameters corresponding to each of the TX-RX location pairs is summarized in Table VI. The format and procedure follow the detailed approach shown for the indoor hotspot environment in [21].

IV. CONCLUSION

We presented an in-depth analysis of radio propagation behavior for InF at 6.75 GHz and 16.95 GHz, based on extensive measurements. 12 TX-RX locations were measured encompassing 5 LOS and 7 NLOS locations spanning 9–38 m. The path loss analysis revealed significant received power even in NLOS scenarios at 6.75 GHz. The PLEs were observed to be small with values below 2 in LOS and close to 2 in NLOS at both 6.75 and 16.95 GHz. The RMS DS was observed to decrease with increasing frequencies in both LOS and NLOS.

The RMS AS also captured showed a decreasing trend with frequency and wide angular spreads were observed particularly in NLOS. Frequency-dependent trends for DS, and AS were observed in contrast to some of the constant modeling currently provided in 3GPP specifications.

REFERENCES

- [1] A. Davidson, “National spectrum strategy implementation plan,” National Telecommunications and Information Administration, Tech. Rep., Mar. 2024.
- [2] S. Kang, M. Mezzavilla, S. Rangan, A. Madanayake, S. B. Venkatakrisnan, G. Hellbourg, M. Ghosh, H. Rahmani, and A. Dhananjay, “Cellular wireless networks in the upper mid-band,” *IEEE Open Journal of the Communications Society*, pp. 1–18, 2024.
- [3] T. S. Rappaport, Y. Xing, O. Kanhere, S. Ju, A. Madanayake, S. Mandal, A. Alkhateeb, and G. C. Trichopoulos, “Wireless communications and applications above 100 GHz: Opportunities and challenges for 6G and beyond,” *IEEE Access*, vol. 7, pp. 78 729–78 757, 2019.
- [4] J. Cheng, W. Chen, F. Tao, and C.-L. Lin, “Industrial IoT in 5G environment towards smart manufacturing,” *Journal of Industrial Information Integration*, vol. 10, pp. 10–19, 2018.
- [5] S. Ju, Y. Xing, O. Kanhere, and T. S. Rappaport, “Millimeter wave and sub-Terahertz spatial statistical channel model for an indoor office building,” *IEEE Journal on Selected Areas in Communications*, vol. 39, no. 6, pp. 1561–1575, 2021.
- [6] T. S. Rappaport, “Characterizing the UHF factory multipath channel,” Ph.D. dissertation, Purdue University, 1987.
- [7] T. S. Rappaport, “Characterization of UHF multipath radio channels in factory buildings,” *IEEE transactions on antennas and propagation*, vol. 37, no. 8, pp. 1058–1069, 1989.
- [8] M. Schmieder, T. Eichler, S. Wittig, M. Peter, and W. Keusgen, “Measurement and characterization of an indoor industrial environment at 3.7 and 28 GHz,” in *2020 14th European Conference on Antennas and Propagation (EuCAP)*. IEEE, 2020, pp. 1–5.
- [9] A. Vijayan, M. Kuhn, J. John, M. Noor-A-Rahim, D. Pesch, B. O’Connor, K. Crean, and E. Armstrong, “5G Wireless Channel Characterization in Indoor Factory Environments: Simulation and Validation,” in *2023 IEEE Wireless Communications and Networking Conference (WCNC)*. IEEE, 2023, pp. 1–6.
- [10] A. Al-Saman, M. Mohamed, M. Cheffena, and A. Moldsvor, “Wideband channel characterization for 6G networks in industrial environments,” *Sensors*, vol. 21, no. 6, p. 2015, 2021.
- [11] Y. Wang, C. Wang, X. Zheng, X. Hao, and X. Liao, “Multi-frequency wireless channel measurements and characterization in indoor industrial scenario,” *IEEE Internet of Things Journal*, 2024.
- [12] E. Lyczkowski, C. Sauer, F. Reichert, and H. Frey, “Power delay profile analysis of industrial channels at 2.1, 2.6, 3.8 and 5.1 GHz,” in *2021 IEEE 32nd Annual International Symposium on Personal, Indoor and Mobile Radio Communications (PIMRC)*. IEEE, 2021, pp. 854–859.
- [13] 3GPP, “Study on channel model for frequencies from 0.5 to 100 GHz (Release 18),” *TR 38.901 V18.0.0 (2024-03)*, pp. 1–98, Mar 2024.
- [14] D. Shakya, T. Wu, M. E. Knox, and T. S. Rappaport, “A Wideband Sliding Correlation Channel Sounder in 65 nm CMOS: Evaluation Board Performance,” *IEEE Transactions on Circuits and Systems II: Express Briefs*, vol. 68, no. 9, pp. 3043–3047, 2021.
- [15] G. R. MacCartney and T. S. Rappaport, “Rural macrocell path loss models for millimeter wave wireless communications,” *IEEE Jnl Sp Ar Comm*, vol. 35, pp. 1663–1677, 2017.
- [16] D. Shakya, M. Ying, T. S. Rappaport, H. Poddar, P. Ma, Y. Wang, and I. Al-Wazani, “Comprehensive FR1(C) and FR3 Lower and Upper Mid-Band Propagation and Material Penetration Loss Measurements and Channel Models in Indoor Environment for 5G and 6G,” *IEEE Open Journal of the Communications Society*, vol. 5, pp. 1–28, 2024.
- [17] D. Shakya *et al.*, “Propagation measurements and channel models in Indoor Environment at 6.75 GHz FR1(C) and 16.95 GHz FR3 Upper-mid band Spectrum for 5G and 6G,” in *(Accepted) IEEE GLOBECOM 2024*, 2024, pp. 1–6.
- [18] D. Shakya *et al.*, “Wideband Penetration Loss through Building Materials and Partitions at 6.75 GHz in FR1(C) and 16.95 GHz in the FR3 Upper Mid-band spectrum,” in *(Accepted) IEEE GLOBECOM 2024*, 2024, pp. 1–6.

TABLE V: Angular Spread Characteristics measured by NYU WIRELESS at 6.75 GHz and 16.95 GHz in LOS and NLOS for the InF environment and Comparison to 3GPP Models [13]

Metric	Condition	6.75 GHz				16.95 GHz			
		NYU	3GPP	$\mathbb{E}(\text{NYU})$	$\mathbb{E}(\text{3GPP})$	NYU	3GPP	$\mathbb{E}(\text{NYU})$	$\mathbb{E}(\text{3GPP})$
Omni RMS I_{gASA} = $\log_{10}(\text{ASA}/1^\circ)$	$\mu_{\text{I}_{\text{gASA}}}^{\text{LOS}}$	1.25	1.62	23.71°	46.56°	1.05	1.55	14.32°	40.86°
	$\sigma_{\text{I}_{\text{gASA}}}^{\text{LOS}}$	0.50	0.31			0.46	0.35		
	$\mu_{\text{I}_{\text{gASA}}}^{\text{NLOS}}$	1.80	1.72	66.38°	58.21°	1.61	1.72	50.40°	58.21°
	$\sigma_{\text{I}_{\text{gASA}}}^{\text{NLOS}}$	0.21	0.30			0.43	0.30		
Omni RMS I_{gASD} = $\log_{10}(\text{ASD}/1^\circ)$	$\mu_{\text{I}_{\text{gASD}}}^{\text{LOS}}$	1.43	1.56	35.89°	39.02°	1.34	1.56	22.91°	39.02°
	$\sigma_{\text{I}_{\text{gASD}}}^{\text{LOS}}$	0.50	0.25			0.20	0.25		
	$\mu_{\text{I}_{\text{gASD}}}^{\text{NLOS}}$	1.64	1.57	45.93°	38.90°	1.49	1.57	34.77°	38.90°
	$\sigma_{\text{I}_{\text{gASD}}}^{\text{NLOS}}$	0.21	0.20			0.32	0.20		

TABLE VI: Large scale spatio-temporal statistics [21]

Freq.	TX	RX	Loc.	TR Sep.	Omni Abs. PL (V-V)	Omni Abs. PL (V-H)	Mean Dir. DS	Omni DS	Mean Lobe ASA	Omni ASA	Mean Lobe ASD	Omni ASD	Mean Lobe ZSA	Omni ZSA	Mean Lobe ZSD	Omni ZSD
[GHz]			[m]	[dB]	[dB]	[ns]	[ns]	[°]	[°]	[°]	[°]	[°]	[°]	[°]	[°]	[°]
6.75	TX1	RX1	LOS	14.6	67.04	80.8	5.9	26.7	6.1	55.2	11.4	31.3	13.5	18.2	11.1	10.7
		RX2	NLOS	16.6	69.81	87.44	8.8	32.7	7.4	50.4	11.0	26.5	7.6	14.8	4.5	11.3
		RX3	NLOS	11.1	67.6	84.32	7.0	23.0	83.8	83.8	14.5	24.4	24.5	24.5	2.6	9.8
		RX4	LOS	9.0	63.12	77.38	13.2	8.0	5.8	5.8	5.9	12.3	5.8	17.9	5.9	13.4
		RX5	NLOS	19.0	71.38	83.26	5.6	27.3	124.0	124.0	18.3	28.2	1.1	7.6	2.9	9.2
	TX2	RX1	LOS	33.3	72.02	89.56	3.0	14.6	7.9	62.1	13.7	41.6	9.3	20.4	1.8	8.9
		RX2	NLOS	38.2	74.82	96.41	4.3	27.9	19.4	75.8	10.4	74.7	3.9	13.8	4.1	11.9
		RX3	LOS	24.9	65.55	87.68	7.5	6.1	6.1	6.1	5.9	6.8	6.1	19.0	5.9	13.4
		RX4	NLOS	24.6	79.06	96.65	13.5	40.5	47.7	47.7	48.2	48.2	12.6	12.6	1.7	5.7
	TX3	RX1	LOS	19.3	65.52	84.35	10.2	18.7	15.2	15.2	15.9	133.3	2.4	13.4	6.1	11.3
		RX2	NLOS	9.5	63.62	82.58	7.6	24.6	28.5	28.5	47.0	57.3	9.5	13.0	2.7	8.8
		RX3	NLOS	14.0	69.85	87.58	4.8	38.6	26.6	78.4	72.0	75.9	13.1	13.3	2.3	7.0
16.95	TX1	RX1	LOS	14.6	74.07	99.07	13.2	17.3	7.7	7.7	7.2	17.2	2.1	7.6	4.1	7.0
		RX2	NLOS	16.6	78.09	104	11.3	56.1	7.5	30.7	9.5	18.6	5.4	9.6	3.9	6.4
		RX3	NLOS	11.1	79.33	99.46	6.0	41.2	9.3	69.4	9.9	17.0	10.8	11.1	2.8	6.1
		RX4	LOS	9.0	73.08	99.45	10.4	8.6	6.7	6.7	7.0	11.7	9.3	9.3	4.0	6.8
		RX5	NLOS	19.0	88.54	116.5	3.3	2.8	5.8	5.8	8.8	10.5	8.9	11.5	2.8	5.9
	TX2	RX1	LOS	33.3	82.63	105.7	8.5	22.0	6.8	71.6	9.6	33.6	7.1	11.8	2.0	5.5
		RX2	NLOS	38.2	86.96	111.9	1.1	11.3	7.0	75.9	7.3	60.7	5.7	13.1	5.4	9.9
		RX3	LOS	24.9	87.31	112.8	5.5	4.7	5.8	5.8	5.6	20.9	5.4	11.5	5.2	8.5
		RX4	NLOS	24.6	90.65	100.7	9.0	43.8	19.5	64.7	14.5	65.6	2.8	6.0	3.6	5.3
	TX3	RX1	LOS	19.3	77.97	98.77	10.9	13.9	8.0	8.0	6.9	35.3	2.2	7.8	1.6	5.1
		RX2	NLOS	9.5	76.09	102.9	5.7	17.4	6.1	29.7	7.6	34.9	4.6	10.8	2.8	5.9
		RX3	NLOS	14.0	82.15	105.6	3.9	50.5	14.1	106.0	15.3	58.5	5.9	7.7	3.8	6.9

- [19] Y. Xing, O. Kanhere, S. Ju, T. S. Rappaport, and G. R. MacCartney, "Verification and calibration of antenna cross-polarization discrimination and penetration loss for millimeter wave communications," in *IEEE VTC*, 2018, pp. 1–6.
- [20] D. Shakya, H. Poddar, and T. S. Rappaport, "A Sub-Terahertz Sliding Correlator Channel Sounder with Absolute Timing using Precision Time Protocol over Wi-Fi," in *IEEE GLOBECOM*, 2023, pp. 1–6.
- [21] T. S. Rappaport, D. Shakya, and M. Ying, "Point data for site-specific mid-band radio propagation channel statistics in the indoor hotspot (InH) environment for 3GPP and Next Generation Alliance (NGA) channel modeling," in *(Submitted) IEEE International Communications Conference (ICC) 2025*, 2025, pp. 1–6.
- [22] D. Shakya *et al.*, "Angular Spread Statistics for 6.75 GHz FR1(C) and 16.95 GHz FR3 Mid-Band Frequencies in an Indoor Hotspot Environment," in *(Submitted) IEEE WCNC 2024*, 2024, pp. 1–6.
- [23] D. Shakya, M. Ying, T. S. Rappaport, P. Ma, I. Al-Wazani, Y. Wu, Y. Wang, D. Calin, H. Poddar, A. Bazzi, M. Chafii, Y. Xing, and A. Ghosh, "Urban Outdoor Propagation Measurements and Channel Models at 6.75 GHz FR1(C) and 16.95 GHz FR3 Upper Mid-band Spectrum for 5G and 6G," in *(Submitted) IEEE International Communications Conference (ICC) 2025*, 2025, pp. 1–6.
- [24] T. S. Rappaport, G. R. MacCartney, M. K. Samimi, and S. Sun, "Wide-band millimeter-wave propagation measurements and channel models for future wireless communication system design," *IEEE Trans. Comm. (invited)*, vol. 63, no. 9, pp. 3029–3056, 2015.
- [25] S. Sun, G. R. MacCartney, M. K. Samimi, and T. S. Rappaport, "Synthesizing omnidirectional antenna patterns, received power and path loss from directional antennas for 5G millimeter-wave communications," in *IEEE GLOBECOM*, 2015, pp. 1–7.
- [26] T. Otim, A. Bahillo, L. E. Díez, P. Lopez-Iturri, and F. Falcone, "Impact of body wearable sensor positions on UWB ranging," *IEEE Sensors Journal*, vol. 19, no. 23, pp. 11 449–11 457, 2019.
- [27] S. Ju, D. Shakya, H. Poddar, Y. Xing, O. Kanhere, and T. S. Rappaport, "142 GHz sub-terahertz radio propagation measurements and channel characterization in factory buildings," *IEEE Transactions on Wireless Communications*, vol. 23, no. 7, pp. 7127–7143, 2024.